Published in final edited form as:
Chem Biol. 2012 July 27; 19(7): 902–912. doi:10.1016/j.chembiol.2012.05.021.

Fluorescent Saxitoxins for Live Cell Imaging of Single Voltage-Gated Sodium Ion Channels beyond the Optical Diffraction Limit

Alison E. Ondrus[1,3], **Hsiao-lu D. Lee**[1,3], **Shigeki Iwanaga**[2], **William H. Parsons**[1], **Brian M. Andresen**[1], **W.E. Moerner**[1], and **J. Du Bois**[1,*]

[1]Department of Chemistry, Stanford University, 333 Campus Drive, Stanford, CA 94305-5080, USA

[2]SYSMEX Corporation, Central Research Laboratories, 4-4-4, Takatsukadai, Nishi-ku, Kobe 651-2271, Japan

SUMMARY

A desire to better understand the role of voltagegated sodium channels (Na_Vs) in signal conduction and their dysregulation in specific disease states motivates the development of high precision tools for their study. Nature has evolved a collection of small molecule agents, including the shellfish poison (+)-saxitoxin, that bind to the extracellular pore of select Na_V isoforms. As described in this report, de novo chemical synthesis has enabled the preparation of fluorescently labeled derivatives of (+)-saxitoxin, STX-Cy5, and STX-DCDHF, which display reversible binding to Na_Vs in live cells. Electrophysiology and confocal fluorescence microscopy studies confirm that these STX-based dyes function as potent and selective Na_V labels. The utility of these probes is underscored in single-molecule and super-resolution imaging experiments, which reveal NaV distributions well beyond the optical diffraction limit in subcellular features such as neuritic spines and filopodia.

INTRODUCTION

Voltage-gated sodium channels (Na_Vs) serve as an obligatory component of the molecular machinery that controls initiation and propagation of action potentials in electrically excitable cells (Caldwell and Levinson, 2004; Catterall, 1992). These integral membrane complexes are expressed as a ~260 kDa pore forming α-subunit with one or two ancillary 33–36 kDa β-proteins. Neuronal activity is shaped in large part by intrinsic differences in the ten known mammalian Na_V α-subtypes and four β-subtypes, their expression levels, tissue distribution, and cellular patterning (Catterall et al., 2005). Not surprisingly, dysregulation of Na_V function is associated with profound pathologies such as neurodegenerative disease, epilepsy, and chronic pain (Catterall et al., 2008). A desire to elucidate the underlying biochemical mechanisms that influence Na_V expression and distribution and to understand how such changes alter signal conduction in neuronal cells motivates the development of molecular tools to probe dynamic processes associated with this protein class.

*Correspondence: jdubois@stanford.edu.
[3]These authors contributed equally to this work

SUPPLEMENTAL INFORMATION

Supplemental Information includes eight figures, one movie, and Supplemental Experimental Procedures and can be found with this article online at http://dx.doi.org/10.1016/j.chembiol.2012.05.021.

Distribution of Na_Vs to discrete cellular locales within a neuron is achieved through a combination of targeted intracellular transport, membrane trafficking, and endocytosis (Leterrier et al., 2010; Catterall, 2010; Dib-Hajj and Waxman, 2010; Cusdin et al., 2008). Na_V clustering at the axon initial segment and nodes of Ranvier plays a key role in action potential generation and saltatory conduction in myelinated nerve cells (Leterrier et al., 2011). Dynamic regulatory pathways also function to tune specific electrophysiological properties of the cell in response to firing activity, neuronal development, myelination, and nerve injury. Recent studies present compelling evidence that functional Na_Vs assemble in sub-diffraction-sized dendritic structures, intimating a multiplicity of functions for these proteins beyond axonal depolarization (Remy et al., 2010). Such data is beginning to reveal how compartmentalization of Na_Vs in cellular substructures can play critical roles in fine-tuning synaptic transmission. Deciphering the mechanisms that impart spatiotemporal control of Na_V distribution is thus tightly entwined with questions of how these channel proteins orchestrate specific neurological processes (Duclohier, 2009). To this end, new technologies for visualizing functional Na_Vs in living cells at the resolution of individual proteins are desired.

Our present understanding of Na_V function at the systems level is shaped by electrophysiology recordings of ionic currents in living cells and immunohistochemical studies on fixed samples (Lorincz and Nusser, 2010; Trimmer and Rhodes, 2004). Although GFP labeling of individual Na_V isoforms presents a viable tool for Na_V visualization (Zimmer et al., 2002a, 2002b; Hallaq et al., 2006), attachment of a fluorescent protein to the Na_V α-subunit has been shown to greatly diminish plasma membrane expression levels and to significantly alter ion conduction properties (Maue, 2007; Baker et al., 2007; Schofield et al., 2008; Ataka and Pieribone, 2002). The latter problem similarly disadvantages use of peptide toxin-based imaging tags to track Na_V dynamics, as does the complex and/or poorly defined binding kinetics of such probes (Massensini et al., 2002; Beaurepaire et al., 2004; Nakada et al., 2003).

Nature has provided a collection of topologically unique guanidinium-derived poisons that bind reversibly and with nanomolar affinity to the outer mouth of the Na_V pore (Figure 1A) (Llewellyn, 2009; Tikhonov and Zhorov, 2011; Scheib et al., 2006). Owing to their exquisite selectivity and favorable on/off kinetics, these molecules are recognized as indispensable tools for electrophysiology. For our purposes, such toxins serve as blueprints for the design of Na_V-selective imaging agents (Strichartz et al., 1995). Herein, we describe the synthesis and characterization of fluorescent small molecules patterned after the paralytic shellfish poison, (+)-saxitoxin (STX) (Andresen and Du Bois, 2009). These reagents enable real-time imaging of native Na_Vs in live cells at the single-molecule level with subdiffraction localization (Lord et al., 2010). The unprecedented spatial and temporal information provided by super-resolution and single particle tracking analysis of these STX-based fluorescent dyes underscores their utility as tools for Na_V study.

RESULTS AND DISCUSSION

Chemical Synthesis of STX-Based Fluorescent Reporter Molecules

Our efforts to develop a preparative route to (+)-STX have furnished an efficient and flexible synthesis of the natural toxin and structural variants, the latter of which are inaccessible by other means. This work has demonstrated that the STX receptor site can accommodate changes to the N21 position of STX (Figure 1A) with minimal loss in affinity between ligand and protein (Andresen and Du Bois, 2009). The availability of STX-NH_3^+ through chemical synthesis offers a convenient starting material from which to append functional groups through mild and selective conjugation strategies (Figure 1B; Figure S1 available online). For our purposes, Cy5 and DCDHF (Lord et al., 2009) fluorophores serve

as bright, photostable, long wavelength emitting probes that, when appropriately derivatized, are soluble and chemically stable in aqueous cell media (Lee et al., 2008). Both Cy5 and DCDHF exhibit high total numbers of emitted photons and large fluorescence quantum yields, and possess absorbance and emission wavelengths that avoid cellular autofluorescence. The use of N-hydroxysuccinimide (NHS) ester derivatives Cy5-NHS (Kvach et al., 2008) and DCDHF-NHS (Wang, 2007) enables "post-synthetic" coupling reactions with STX-NH_3^+ to furnish STX-fluorophore conjugates STX-Cy5 and STX-DCDHF (STX-Cy5, $\lambda_{abs/em}$ = 655/665 nm; STX-DCDHF, $\lambda_{abs/em}$ = 580/640 nm in H_2O; Figure S2A). Purification by reverse-phase HPLC affords the corresponding trifluoroacetate salts of these compounds as water soluble blue and violet powders, respectively, which can be stored for several months at −20°C when shielded from light.

Electrophysiological Characterization of Na_V Block by STX, STX-Cy5, and STX-DCDHF

In order to assess the potency and binding kinetics of STX-based fluorescent probes, we have conducted whole-cell voltageclamp electrophysiological studies with rat pheochromocytoma 12 (PC12) cells. This cell type finds extensive use as a model for neuronal differentiation (Vaudry et al., 2002). Exposure of PC12 cells to nerve growth factor (NGF) over a period of days induces expression of STX-sensitive isoforms $Na_V1.7$ (Toledo-Aral et al., 1997) and $Na_V1.2$ (Mandel et al., 1988), and engenders characteristics that include neurite extension, suspended proliferation, and gated ion current (Greene and Tischler, 1976).

Prior efforts to measure the affinity of STX toward endogenous Na_Vs in NGF-treated PC12 cells have employed ^{3}H-STX to determine an apparent K_d in the low nanomolar range (3.0 ± 0.5 nM) (Rudy et al., 1982). Consistent with the nanomolar K_d for STX, whole-cell voltage-clamp recordings obtained after 4–7 day treatment with NGF give an IC_{50} for STX of 2.1 ± 0.2 nM (Figure 1C). Significantly, IC_{50} values of 40 ± 3 and 106 ± 23 nM determined for STX-Cy5 and STX-DCDHF, respectively, are within 1.5 orders of magnitude of the parent toxin. These results are commensurate with an STX binding model that orients N21 toward extracellular space (Andresen and Du Bois, 2009). As with the parent toxin, block by both STX conjugates is fully reversible, and peak Na^+ ion current is restored upon perfusion of the patched cell with buffer solution (Figure S3).

Fluorescent Labeling of Na_Vs by STX-Cy5 and STX-DCDHF

We have evaluated the specificity of STX probe binding to Na_Vs in NGF-differentiated PC12 cells through Na_V antibody colocalization experiments. Confocal images were obtained on cells exposed to phosphate buffered saline solutions of 10 nM STX-Cy5 or 15 nM STX-DCDHF. Overlap analysis following cell fixation, membrane permeabilization, and sequential staining with a pan-Na_V antibody/Alexa488-conjugated secondary antibody and STX-Cy5 or STX-DCDHF (Figures 2G–2L) yields Manders coefficients of 0.94 ± 0.02 and 0.93 ± 0.08, respectively. The excellent correspondence of these dyes with Alexa488-conjugated antibody staining offers compelling support that modified STXs selectively target Na_V proteins (see also Supplemental Experimental Procedures).

Preblocking experiments with saturating concentrations of STX (10 μM) give additional evidence for Na_V labeling by STX-Cy5 and STX-DCDHF. Cells treated with STX prior to application of either dye conjugate show low levels of fluorescence at the extracellular membrane, as determined by confocal imaging (Figures 2A, 2B and S4A). These results are consistent with STX occupancy of the Na_V outer pore precluding association of the fluorescent STX probes.

As a final control to assess the specificity of Na_V labeling by STX-Cy5 and STX-DCDHF, we have performed both confocal and wide-field single-molecule imaging experiments on Chinese hamster ovary (CHO) cells transfected with a plasmid encoding for the α -subunit of rat $Na_V1.4$ ($rNa_V1.4$). Previous work in our group has established the ability of modified STX derivatives to effect channel block with this construct, which shows 70% sequence homology to $Na_V1.2$ and 71% sequence homology to $Na_V1.7$ expressed in PC12; all three rat isoforms share a similar p-loop sequence that defines the STX binding site (Figure S5C). Both ensemble and single-molecule images of native CHO cells in the presence of STX-Cy5 or STX-DCDHF show no fluorescence emission from the cytoplasmic membrane or from within the cell. By contrast, membrane localization of the dyes is readily evident in CHO cells transfected with $rNa_V1.4$ (Figures S5A and S5B; see also Supplemental Experimental Procedures). These data provide strong corroborating support for the selective association of STX-dye conjugates with Na_Vs.

Confocal Imaging of Na_V Distribution in PC12 Cells

The cellular distribution of Na_Vs in live cells has been explored indirectly through voltage-clamp measurements. These data show increased sodium ion current density in excised neurites relative to the cell body of intact cells (O'Lague et al., 1985). Corresponding immunocytology experiments to mark the location of Na_Vs in NGF-differentiated PC12 cells appear in a single report (Toledo-Aral et al., 1997). Such images are obtained with a specific antibody raised against NGF-induced $Na_V1.7$ and reveal upregulated channel populations in neurite growth cones and in the membrane of the cell soma. In accord with these findings, confocal images obtained with STX-Cy5 and STX-DCDHF against NGF-treated PC12 cells highlight specific labeling of Na_Vs at neuritic processes and in the somatic membrane (Figures 2G–2L). Regions of enhanced fluorescence intensity are focused at growth cones and in the periphery of the cell body, data that concurs with recent reports describing clustering of Na_Vs in unmyelinated neurons (England et al., 1990; Henry et al., 2006, Zeng and Tang, 2009).

In confocal experiments performed with sub-IC_{50} concentrations of STX-Cy5 and STX-DCDHF (10 and 15 nM, respectively), membrane-associated STX-fluorophores are clearly visible above the background emission of the unbound probe. This unique brightness enhancement is especially pronounced with STX-DCDHF (Lord et al., 2009) (Figure S2B). Z-stack cross sections acquired at multiple time points over 15 min to 6 hr reveal that fluorescence is restricted to the cell surface, a finding that demonstrates STX-Cy5 and STX-DCDHF neither passively diffuse across the cell membrane nor activate internalization pathways (Figure S4D). When cells are incubated in media containing STX-fluorophore, imaging experiments can be performed in an incubator-equipped microscope over several days with no observable deleterious effect on cell morphology or viability. Consistent with a reversible ligand-protein binding interaction, the fluorescence signal from either probe is effectively washed-off the cell by replacement of the medium (Figures 2C, 2D, and S4B). The time course for fluorescence intensity decay in these experiments is within the same order of magnitude as the off-rate kinetic measurements from electrophysiology recordings (Figures S3 and S6).

Transcriptional profiling and electrophysiology data suggest that a measurable level of Na_Vs exists in the plasma membrane of undifferentiated PC12 cells (Mandel et al., 1988). To query the effect of NGF treatment on Na_V expression, we have compared the integrated fluorescence intensity of STX-Cy5 and STX-DCDHF in identical populations of PC12 cells cultured with and without NGF (4–7 days). Undifferentiated cells exposed to 10 nM STX-Cy5 or 15 nM STX-DCDHF show uniform fluorescence emission at the outer membrane with average intensities of ~20% relative to NGF-treated cells (Figures 2E, 2F, and S4C). These findings are in agreement with Na_V occurrence in undifferentiated cells and reflect

the substantial upregulation in protein expression caused by NGF (Ginty et al., 1992; Toledo-Aral et al., 1995; Hilborn et al., 1998). The ability to detect small basal populations of Na_Vs in live cells could help further our understanding of how posttranslational protein modification is used to regulate neuronal cellular plasticity (Cantrell and Catterall, 2001).

Single Particle Tracking of Na_Vs in the Somatic Membrane and Measurement of Instantaneous Na_V Velocities in Neurites

In principle, single-molecule tracking analysis can differentiate among physical processes associated with Na_V behavior, including membrane diffusion, cytoskeleton-associated transport, and endocytotic turnover (Matsuoka et al., 2009; Kusumi et al., 2010). Such experiments can also distinguish between populations of Na_Vs that reside permanently in a distinct state or represent dynamic transitions of a single population—information unavailable through ensemble imaging (Vrljic et al., 2009). We have employed STX-Cy5 and STX-DCDHF in single particle tracking experiments and instantaneous velocity measurements to characterize the motion of individual Na_Vs in NGF-differentiated PC12 cells. The availability of fluorescent markers that preserve the motility of Na_Vs is paramount for this type of study, favoring the use of small molecule dyes over fluorescent fusion protein constructs. We have capitalized on the longer residence binding time of STX-DCDHF relative to STX-Cy5 in the plasma membrane of PC12 cells to examine single-molecule Na_V tracks on the somatic surface (vide infra).

Single 50 ms epifluorescence imaging frames of differentiated PC12 cells obtained in the presence of STX-DCDHF clearly show individual Na_Vs on the somatic membrane. Throughout this region, small clusters of Na_Vs are also observed (Figure 3B). Illustrative tracks of single molecules plotted versus time reveal heterogeneous trajectories that are characteristic of confined diffusion, Brownian motion, and directed transport (Qian et al., 1991) (Figure 3D). Although exhaustive analysis of the modes of motion of Na_V is beyond the scope of this report, for the purposes of a preliminary characterization, ~4,000 single Na_Vs in the somatic membrane were tracked using 12.8 nM STX-DCDHF at low imaging intensity to reduce photobleaching. As revealed by these data, labeled Na_Vs in the membrane of the soma exhibit an average visibility time of 250 ±7 ms and display multiple trajectories before disappearing. Selection of 370 trajectories with 10 steps or more allowed us to compute short-time diffusion coefficients from mean square displacements. The measured D distribution was analyzed under the assumption that all recorded values arise from underlying random Brownian motion characterized by a single diffusion coefficient, D_0, which yields a well-known probability distribution (see also Supplemental Experimental Procedures). The expected distribution is designated by the smooth red curve (Figure 3C), with the average diffusion coefficient, $D_{avg} = 0.036 \pm 0.027\ \mu m^2/s$ (N = 370) taken as D_0. Departures from the smooth curve indicate heterogeneous motion, as observed (Figure 3C). The measured diffusion coefficients are comparable to reported values for Na_Vs restricted to specific membrane regions in neurons (Leterrier et al., 2010; Nakada et al., 2003; Brachet et al., 2010).

Analysis of the trajectories of single Na_Vs in neuritic projections of differentiated PC12 cells at 100 ms temporal resolution is made possible by capitalizing on the prolonged visibility time of STX-DCDHF at the cell membrane (Figure 3E). Tracking instantaneous velocity of five individually resolved Na_Vs undergoing directed motion affords lower and upper speed limits of 680 and 970 ± 10 nm/s (59 mm/day and 85 mm/day), respectively, along the length of the neurite. These values are consistent with reported rates of intracellular axonal transport of certain neuronal proteins and vesicles (Brown, 2003).

Single-Molecule Imaging of Na_V Dynamics in Filopodia Extension and Retraction

The ability to spatially resolve single molecules in the dynamic environment of a living cell permits real-time tracking of the distribution of molecules over a small region of interest. In the cellular membrane, where the motion of labeled proteins is restricted to two dimensions, changing fluorescence patterns can be used to trace morphological fluctuations in these structures. Here, rapid photobleaching of Na_V bound STX-Cy5 affords a visibility time of 100 ± 10 ms (Figures 4I and Figure S8A; see also Supplemental Experimental Procedures). This short visibility time is well suited for rapid stochastic sampling of single Na_V locations within filopodia of differentiated PC12 cells (Figures 4C–4G). Locations of individual Na_Vs can be summed into a single image by maxplotting the data, a method in which the highest intensity value of an individual pixel over a fixed time interval is taken to be the value of that pixel (Figures 4C–4G and S7A). In this manner, Na_V spatial distribution can be used to outline growth cone motility of cellular filopodia at a temporal resolution of 10 s. Analysis over a 24 min period reveals dynamic growth and retraction of filopodia at a maximum extension/retraction rate of 360 nm/s with an average value of 80 ± 90 nm/s (Figures 4H and Figure S7C). Notably, the observed rates are commensurate with previously determined traction rates measured in neurons (Mallavarapu and Mitchison, 1999; Lu et al., 1997; Sheetz et al., 1992; Kress et al., 2007; Costantino et al., 2008; Laishram et al., 2009). These rapid, noncontinuous motions are reminiscent of the sliding of actin filaments (Mallavarapu and Mitchison, 1999) and suggest that analogous cytoskeleton associated mechanisms may play a significant role in the trafficking of filopodial Na_Vs.

Super-Resolution Imaging of Na_Vs in Neuritic Spines and Filopodia

The small dimensions of neuritic spines and filopodia in NGF-differentiated PC12 cells render the study of protein dynamics intractable by conventional diffraction-limited confocal or epifluorescence microscopy. Super-resolution imaging of individual proteins thus has the potential to reveal fine details of Na_V locations within these intricate substructures, information that may give deeper insight into integrated channel function. Pointillist super-resolution reconstruction relies on efficient turn-on/turn-off fluorescence in order to maintain sparse populations of emitters from Na_Vs within the region of interest. While both saxitoxins afford efficient on/off fluorescence necessary for super-resolution imaging, STX-Cy5 exhibits a shorter visibility time and is particularly well suited for such experiments. Photophysical analysis reveals that turn-off of the STX-Cy5 fluorescence signal is primarily caused by intensity-dependent photobleaching of the dye molecule (Figures S8D and S8E). By carefully selecting pump laser intensities and exposure times, background emission of the unbound probe is negligible and single Na_Vs blocked by the STX probes are clearly visible (signal/ background STX-Cy5 = 1.8 ± 0.4, STX-DCDHF = 4.2 ± 0.5; see also Supplemental Experimental Procedures). With optimized imaging parameters, experiments can be performed with a fixed concentration of either STX-fluorophore in the cell medium, thus allowing continuous turn-on events to occur with the binding of new dye molecules (Figures S8A–S8C). As such, these experiments can be performed in the absence of thiol reductants or photostimulation. We view this method as a target-specific variation of points accumulation for imaging in nanoscale topography (PAINT) (Sharonov and Hochstrasser, 2006), which provides a sampling of Na_V locations within these morphological structures.

Harnessing the short visibility time of STX-Cy5 enables the recording of multiple single Na_V positions to yield pointillist super-resolution reconstruction with a mean statistical localization precision of 25 ± 3 nm (Figures S8F and S8G). Under these conditions, an imaging time of 5 s, averaging 5,300 ± 200 localizations/s, is needed to accumulate sufficient data to create a well defined ~300 μm^2 image of the neuritic structure (Figure 5A). As each single-molecule localization event is represented by a Gaussian with fixed width and amplitude, this data also reflects the relative densities of Na_Vs in different cellular

regions. The reconstructed images show punctate populations of Na_Vs at nodes along the neurite shaft and at the origins of numerous projections extending from the neurite body. Neuritic spines, ~85 nm in width, are perceptible as discrete structures containing Na_Vs distributed both individually and in small clusters (Figures 5D, 5F, and 5J). A quasi-real-time super-resolution movie generated using a weighted moving average algorithm reveals that these neuritic outgrowths exhibit highly fluxional lateral movements, extensions, and retractions on the timescale of hundreds of milliseconds (Figure 5L; Movie S1). These rates, on par with dendritic spine motility in neurons (Bhatt et al., 2009), enable us to visualize at nanometer precision and in quasi-real-time structural changes and specific Na_V distributions in motile neuritic spines.

SIGNIFICANCE

An intricate array of regulatory networks and dynamic trafficking mechanisms control the patterning of Na_V subtypes and shape the specific conductive properties of a cell. Despite the importance of Na_Vs in neuronal function, methods for live cell imaging of these proteins are conspicuously few. Saxitoxin offers a unique molecular template for the design of new pharmacological and imaging agents to interrogate dynamic channel function. The singular power of chemical synthesis has made possible access to fluorescently-labeled forms of STX that maintain high affinity to the channel and reversible binding kinetics. We have described the electrophysiological characterization of these toxin conjugates and have demonstrated their utility for live-cell imaging of Na_Vs in NGF-treated PC12 cells. Our results further highlight the potential for STX-Cy5 and STX-DCDHF to detect small populations of Na_Vs in undifferentiated PC12 cells. The unique properties of these probes have been underscored in single-molecule imaging and super-resolution experiments. Such data provide analysis of Na_V motility in functionally distinct regions of the excitable cell membrane and quasi-real-time super-resolution visualization of changing Na_V populations in neuritic spines. These studies form part of a larger program dedicated to elucidating dynamic processes associated with Na_V function and their integral role in bioelectrical conduction.

EXPERIMENTAL PROCEDURES

Synthetic Procedures and Characterization Data

Caution—Saxitoxin derivatives are expected to show similar toxicity and symptomatology to saxitoxin, tetrodotoxin, and other sodium channel blockers and should be handled with appropriate care for safety.

Synthesis of STX-Cy5

To a solution of STX-NH_3^+ (6.6 mg, 6.4 μmol) in 635 μl of a 2:1 mixture of MeCN/pH 9.5 buffer (0.1 M aqueous $NaHCO_3/Na_2CO_3$) was added Cy5-NHS (5.8 mg, 9.4 μmol, 1.5 equivalent) (Figure 1B). The mixture was stirred at room temperature for 2 hr, then acidified with 3.0 ml of 0.10% aqueous CF_3CO_2H. After concentrating this solution under reduced pressure, the solid material was purified by reverse phase HPLC (Altima C18, 10 μm, 10 × 250 mm column, eluting with a gradient flow over 30 min of 20:80 MeCN/ H_2O with 0.1% CF_3CO_2H → 50:50 MeCN/$H_2$0 with 0.1% CF_3CO_2H, 254 nm ultraviolet [UV] detection). At a flow rate of 6 ml/min, STX-Cy5 had a retention time of 26.0 min and was isolated following lyophilization as a dark blue solid (2.7 mg, 36%).

Synthesis of STX-DCDHF

To a solution of STX-NH_3^+(3.1 mg, 3.0 μmol) in 150 μl of a 3:1 mixture of MeCN/ pH 9.5 buffer (0.1 M aqueous $NaHCO_3/Na_2CO_3$) was added DCDHF-NHS (3.0 mg, 5.9 μmol, 2.0

equivalent) (Figure 1B). The reaction was stirred at room temperature for 3 hr, then acidified with 40 μl of 1.0 N aqueous HCl. After concentrating this solution under reduced pressure, the solid material was purified by reverse phase HPLC (Altima C18, 10 μm, 10 × 250 mm column, eluting with a gradient flow over 30 min of 20:80 MeCN/H_2O with 0.1% CF_3CO_2H → 80:20 MeCN/H_20 with 0.1% CF_3CO_2H, 254 nm UV detection). At a flow rate of 6 ml/min, STX-DCDHF had a retention time of 14.6 min and was isolated following lyophilization a dark violet solid (1.3 mg, 44%).

Cell Culture

PC12 (pheochromocytoma 12) cells were grown in DMEM phenol red-free media (GIBCO BRL, Grand Island, NY) supplemented with 10% horse serum (GIBCO BRL), 5% fetal calf serum (HyClone, Logan, UT), and 100 U/ml pen-strep (GIBCO BRL). Cells were grown in a 5% carbon dioxide, 96% relative humidity incubator at 37°C, and passaged every ~3 days. Passaging of cells was accomplished by careful aspiration of media, treatment with 1 ml of trypsin-EDTA (0.05%, Invitrogen, Carlsbad, CA) for ~5 min until full dissociation of cells from the plate surface was observed, and dilution with 4 ml of growth medium. Approximately 1 ml of this suspension was then diluted in 9 ml growth medium in a new 10 cm plate. For electrophysiological recordings or microscopy experiments involving differentiated PC12 cells, 100 ng/ml of nerve growth factor (NGF; BD Biosciences, Bedford, MA) was added 1–7 days prior to data collection. Media was replaced every 3 days.

CHO cell culture was performed as described previously (Andresen and Du Bois, 2009). Transfection with rat $Na_V1.4$ ($rNa_V1.4$) and eGFP was accomplished using the calcium phosphate precipitation method or the Lipofectamine method.

Electrophysiology

Acquisition Protocols—Sodium currents were measured using the patch-clamp technique in the whole-cell configuration with an Axopatch-200b amplifier (Axon Instruments, Union City, CA). Borosilicate glass micropipettes (Sutter Instruments, Novato, CA) were fire-polished to a tip diameter yielding a resistance of 1.0–3.0 MΩ in the working solutions. Pipettes were filled with (in mM): CsCl 140, KCl 1, EGTA 1, HEPES 10, and the pH was adjusted to 7.2 with solid CsOH (D'Arcangelo et al., 1993). The external solution had the following composition (in mM): NaCl 140, $CaCl_2$ 1, HEPES 10, and the pH was adjusted to 7.4 with solid CsOH.

The output of the patch-clamp amplifier was filtered with a built-in low-pass, four-pole Bessel filter having a cutoff frequency of 10 kHz and sampled at 100 kHz. The membrane was kept at a holding potential of −100 mV. Pulse stimulation and data acquisition used 16 bit D–A and A–D converters (Axon Instruments Digidata 1322A) controlled with the PClamp software (Axon Instruments). Leak currents were subtracted using a standard P/4 protocol of the same polarity. Access resistance was always <4 MΩ and the cell capacitance was between 4 and 20 pF, as measured by the compensating circuit of the amplifier. All measurements were done at room temperature (20–22°C). Recordings were made at least 5 min after establishing the whole-cell and voltage-clamp configuration to allow for stabilization of the voltage-dependent properties of the channels. Currents were elicited by 10 ms step depolarizations from a holding potential of −100 to 0 mV.

Stock solutions of STX-Cy5 and STX-DCDHF were prepared by serial dilution with external solution and stored at 4°C in the dark. PC12 cells were grown and differentiated on glass coverslips (5 mm #1 thickness, Warner Instruments, Hamden, CT) placed on the bottom surface of a culture dish and coverslips were removed just prior to recording. Current

measurements were recorded under continuous perfusion, controlled manually by syringe addition.

Data Analysis—Data were fitted to Langmuir isotherms according to the equation:

$$\frac{I}{I_o} = 1 - \left(\frac{[\text{toxin}]}{(IC_{50} + [\text{toxin}])} \right),$$

where I / I_o is the fraction of remaining current, [toxin] is the concentration of STX or STX-fluorophore, and IC_{50} is the concentration of STX or STX-fluorophore that effects 50% current block. Custom software developed in the Igor Pro environment (Wavemetrics) was used to determine IC_{50} values expressed as mean ± 1 SD.

Confocal and Wide-Field Epifluorescence Microscopy

Instrumentation—Confocal images were acquired at the Cell Sciences Imaging Facility (Stanford University) on a Zeiss LSM 510 Confocal Laser Scanning Module mounted on a Zeiss Axiovert 200M inverted microscope using either a LCI Plan-Neofluar 25 × /0.8 l mm Korr DIC objective or an A-Plan-Apochromat 63 × /1.4 Oil DIC objective. Cy5 and DCDHF chromophores were excited at 633 nm with a 5 mW HeNe laser at 10%–15% output; emission was detected through a HFT UV/488/543/633 dichroic beam splitter with a 650 nm long-pass filter. Alexa488 was excited at 488 nm with a 25 mW Argon laser at 10% output, and emission was detected through a HFT 488 dichroic beam splitter with a 500–550 nm IR bandpass filter.

Sample Preparation—PC12 cells were plated on glass bottom dishes (MatTek Corp, Ashland, MA) and induced to differentiate with NGF (unless otherwise noted) for 1–7 days. Prior to data collection, cells were washed with PBS and incubated in media consisting of phenol red-free DMEM containing 10% CCS, 1:100 v/v pen-strep, and 100 ng/ml NGF as indicated. Stock solutions of STX-Cy5 or STX-DCDHF in <100 μl PBS were added to final concentrations of 10 nM or 15 nM, respectively.

Single-Molecule and Super-Resolution Microscopy

Instrumentation—Both transmission images of the cells and epifluorescence images of single molecules were acquired using an inverted microscope (IX71, Olympus, Center Valley, PA). Bright field illumination from a condenser allowed for visualization of the edges of the cells. Fluorescence imaging of the cells was performed with wide-field epi-illumination in an area of ~42 μm × 42 μm. Because the mechanical drift of the stage (Semprex, Campbell, CA) was negligible during the recording time a fiduciary correction was not necessary. Laser illumination at 633 nm afforded an intensity of ~200 W/cm^2 at the sample plane for Cy5 chromophore imaging. Laser illumination at 594 nm provided an intensity of ~40 W/cm^2 at the sample plane for DCDHF chromophore imaging. Epifluorescence images were collected with a 60× magnification, 1.45 NA, oil-immersion objective (PlanApo, Olympus, Center Valley, PA) and imaged through a 640 nm long-pass filter and a 635 nm dichroic mirror (Omega Optical, Brattleboro, VT) for images acquired with 633 nm excitation, and a 595 dichroic mirror and 615 long-pass filter were used for images acquired with 594 nm excitation. An EMCCD-camera (IXonDV887, Andor, South Windsor, CT) was used for data collection. The pumping beam intensity was adjusted with neutral density filters to give an acceptable signal-to-background ratio while minimizing fluorophore bleaching. During data collection samples were housed in a Tokai Hit thermo incubator (Tokai Hit, Japan) maintained at 37°C with 5% CO_2 that was fixed to a Semprex precision stage using a custom machined adaptor.

Sample Preparation—Borosilicate coverglass coated with collagen (Nalge Nunc International, Naperville, IL) was treated with 50 μg/ml fibronectin (human plasma, Calbiochem, San Diego, CA) in PBS at pH 7.4 for 1 hr at room temperature prior to deposition of cells. PC12 cells were plated and induced to differentiate with NGF for 1–7 days. Prior to imaging, cells were washed with PBS and placed in phenol red-free DMEM containing 100 ng/ml NGF and STX-DCDHF (13 nM) or STX-Cy5 (3 nM or 10 nM).

Data Analysis—Trajectories of single conjugates (Figure 3) were extracted using a Single Particle Tracking program from ETH-Zurich. Maxplot images (Figure 4) were obtained from raw image stacks using ImageJ function Z Project with maximum intensity. Super-resolution reconstructions (Figure 5) were made possible by using super-localization fitting to determine subdiffraction single-molecule locations (Biteen et al., 2008) and final reconstructions utilized a custom macro written in ImageJ, where each single molecule was represented as a two-dimensional Gaussian having a constant amplitude and σ (SD) equal to the average statistical error of the center of the fit, i.e., 30 nm.

Supplementary Material

Refer to Web version on PubMed Central for supplementary material.

Acknowledgments

A.E.O., H.L., S.I., B.M.A., W.E.M., and J.D. designed research; A.E.O., H.L., S.I., and W.H.P. performed research; A.E.O., H.L., and S.I. analyzed data; and A.E.O., H.L., W.E.M., and J.D. wrote the paper. The authors thank Professor R.J. Twieg and J.C. Williams for the gift of DCDHF-NHS. We are grateful to Professor Merritt Maduke for allowing use of her electrophysiology equipment and for many helpful discussions. This work was supported in part by R01-GM086196 (to W.E.M.) and R01-NS45684 (to J.D.) from the National Institute of General Medical Sciences and the National Institute of Neurological Disorders and Stroke, respectively, and by a grant from the Tobacco-Related Disease Research Program (to J.D.). W.H.P. is the recipient of a Stanford Interdisciplinary Graduate Fellowship. J.D. is a cofounder of SiteOne Therapeutics, Inc.

REFERENCES

Andresen BM, Du Bois J. De novo synthesis of modified saxitoxins for sodium ion channel study. J. Am. Chem. Soc. 2009; 131:12524–12525. [PubMed: 19678702]

Ataka K, Pieribone VA. A genetically targetable fluorescent probe of channel gating with rapid kinetics. Biophys. J. 2002; 82:509–516. [PubMed: 11751337]

Baker BJ, Lee H, Pieribone VA, Cohen LB, Isacoff EY, Knopfel T, Kosmidis EK. Three fluorescent protein voltage sensors exhibit low plasma membrane expression in mammalian cells. J. Neurosci. Methods. 2007; 161:32–38. [PubMed: 17126911]

Beaurepaire E, Buissette V, Sauviat M-P, Giaume D, Lahlil K, Mercuri A, Casanova D, Huignard A, Martin J-L, Gacoin T, et al. Functionalized fluorescent oxide nanoparticles: artificial toxins for sodium channel targeting and imaging and the single-molecule level. Nano Lett. 2004; 4:2079–2083.

Bhatt DH, Zhang S, Gan W-B. Dendritic spine dynamics. Annu. Rev. Physiol. 2009; 71:261–282. [PubMed: 19575680]

Biteen JS, Thompson MA, Tselentis NK, Bowman GR, Shapiro L, Moerner WE. Super-resolution imaging in live Caulobacter crescentus cells using photoswitchable EYFP. Nat. Methods. 2008; 5:947–949. [PubMed: 18794860]

Brachet A, Leterrier C, Irondelle M, Fache MP, Racine V, Sibarita JB, Choquet D, Dargent B. Ankyrin Grestrictsion channel diffusion at the axonal initial segment before the establishment of the diffusional barrier. J. Cell Biol. 2010; 191:383–395. [PubMed: 20956383]

Brown A. Axonal transport of membranous and nonmembranous cargoes: a unified perspective. J. Cell Biol. 2003; 160:817–821. [PubMed: 12642609]

Caldwell, JH.; Levinson, SR. The biology of voltage-gated sodium channels. In: Maue, MA., editor. Molecular Insights into Ion Channel BiologyinHealth and Disease. San Diego, CA: Elsevier; 2004. p. 15-50.

Cantrell AR, Catterall WA. Neuromodulation of Na^+ channels: an unexpected form of cellular plasticity. Nat. Rev. Neurosci. 2001; 2:397–407. [PubMed: 11389473]

Catterall WA. Cellular and molecular biology of voltage-gated sodium channels. Physiol. Rev. 1992; 72(4 Suppl):S15–S48. [PubMed: 1332090]

Catterall WA. Signaling complexes of voltage-gated sodium and calcium channels. Neurosci. Lett. 2010; 486:107–116. [PubMed: 20816922]

Catterall WA, Goldin AL, Waxman SG. International Union of Pharmacology. XLVII. Nomenclature and structure-function relationships of voltage-gated sodium channels. Pharmacol. Rev. 2005; 57:397–409. [PubMed: 16382098]

Catterall WA, Dib-Hajj SD, Meisler MH, Pietrobon D. Inherited neuronal ion channelopathies: new windows on complex neurological diseases. J. Neurosci. 2008; 28:11768–11777. [PubMed: 19005038]

Costantino S, Kent CB, Godin AG, Kennedy TE, Wiseman PW, Fournier AE. Semi-automated quantification of filopodial dynamics. J. Neurosci. Methods. 2008; 171:165–173. [PubMed: 18394712]

Cusdin FS, Clare JJ, Jackson AP. Trafficking and cellular distribution of voltage-gated sodium channels. Traffic. 2008; 9:17–26. [PubMed: 17988224]

D'Arcangelo G, Paradiso K, Shepherd D, Brehm P, Halegoua S, Mandel G. Neuronal growth factor regulation of two different sodium channel types through distinct signal transduction pathways. J. Cell Biol. 1993; 122:915–921. [PubMed: 8394370]

Dib-Hajj SD, Waxman SG. Isoform-specific and pan-channel partners regulate trafficking and plasma membrane stability; and alter sodium channel gating properties. Neurosci. Lett. 2010; 486:84–91. [PubMed: 20817075]

Duclohier H. Structure-function studies on the voltage-gated sodium channel. Biochim. Biophys. Acta. 2009; 1788:2374–2379.

England JD, Gamboni F, Levinson SR, Finger TE. Changed distribution of sodium channels along demyelinated axons. Proc. Natl. Acad. Sci. USA. 1990; 87:6777–6780. [PubMed: 2168559]

Ginty DD, Fanger GR, Wagner JA, Maue RA. The activity of cAMP-dependent protein kinase is required at a posttranslational level for induction of voltage-dependent sodium channels by peptide growth factors in PC12 cells. J. Cell Biol. 1992; 116:1465–1473. [PubMed: 1311713]

Greene LA, Tischler AS. Establishment of a noradrenergic clonal line of rat adrenal pheochromocytoma cells which respond to nerve growth factor. Proc. Natl. Acad. Sci. USA. 1976; 73:2424–2428. [PubMed: 1065897]

Hallaq H, Yang Z, Viswanathan PC, Fukuda K, Shen W, Wang DW, Wells KS, Zhou J, Yi J, Murray KT. Quantitation of protein kinase A-mediated trafficking of cardiac sodium channels in living cells. Cardiovasc. Res. 2006; 72:250–261. [PubMed: 16973141]

Henry MA, Freking AR, Johnson LR, Levinson SR. Increased sodium channel immunofluorescence at myelinated and demyelinated sites following an inflammatory and partial axotomy lesion of the rat infraorbital nerve. Pain. 2006; 124:222–233. [PubMed: 16828970]

Hilborn MD, Vaillancourt RR, Rane SG. Growth factor receptor tyrosine kinases acutely regulate neuronal sodium channels through the src signaling pathway. J. Neurosci. 1998; 18:590–600. [PubMed: 9425001]

Kress H, Stelzer EHK, Holzer D, Buss F, Griffiths G, Rohrbach A. Filopodia act as phagocytic tentacles and pull with discrete steps and a load-dependent velocity. Proc. Natl. Acad. Sci. USA. 2007; 104:11633–11638. [PubMed: 17620618]

Kusumi A, Shirai YM, Koyama-Honda I, Suzuki KGN, Fujiwara TK. Hierarchical organization of the plasma membrane: investigations by single-molecule tracking vs. fluorescence correlation spectroscopy. FEBS Lett. 2010; 584:1814–1823. [PubMed: 20178787]

Kvach MV, Ustinov AV, Stepanova IA, Malakhov AD, Skorobogatyi MV, Shmanai VV, Korshun VA. A convenient synthesis of cyanine dyes: reagents for the labeling of biomolecules. Eur. J. Org. Chem. 2008; 2008:2107–2117.

Laishram J, Avossa D, Shahapure R, Torre V. Mechanical computation in neurons. Dev. Neurobiol. 2009; 69:731–751. [PubMed: 19593765]

Lee HL, Dubikovskaya EA, Hwang H, Semyonov AN, Wang H, Jones LR, Twieg RJ, Moerner WE, Wender PA. Single-molecule motions of oligoarginine transporter conjugates on the plasma membrane of Chinese hamster ovary cells. J. Am. Chem. Soc. 2008; 130:9364–9370. [PubMed: 18578528]

Leterrier C, Brachet A, Fache M-P, Dargent B. Voltage-gated sodium channel organization in neurons: protein interactions and trafficking pathways. Neurosci. Lett. 2010; 486:92–100. [PubMed: 20817077]

Leterrier C, Brachet A, Dargent B, Vacher H. Determinants of voltage-gated sodium channel clustering in neurons. Semin. Cell Dev. Biol. 2011; 22:171–177. [PubMed: 20934527]

Llewellyn LE. Sodium channel inhibiting marine toxins. Prog. Mol. Subcell. Biol. 2009; 46:67–97. [PubMed: 19184585]

Lord SJ, Conley NR, Lee HL, Nishimura SY, Pomerantz AK, Willets KA, Lu Z, Wang H, Liu N, Samuel R, et al. DCDHF fluorophores for single-molecule imaging in cells. ChemPhysChem. 2009; 10:55–65. [PubMed: 19025732]

Lord SJ, Lee H-L, Moerner WE. Single-molecule spectroscopy and imaging of biomolecules in living cells. Anal. Chem. 2010; 82:2192–2203. [PubMed: 20163145]

Lorincz A, Nusser Z. Molecular identity of dendritic voltage-gated sodium channels. Science. 2010; 328:906–909. [PubMed: 20466935]

Lu M, Witke W, Kwiatkowski DJ, Kosik KS. Delayed retraction of filopodia in gelsolin null mice. J. Cell Biol. 1997; 138:1279–1287. [PubMed: 9298983]

Mallavarapu A, Mitchison T. Regulated actin cytoskeleton assembly at filopodium tips controls their extension and retraction. J. Cell Biol. 1999; 146:1097–1106. [PubMed: 10477762]

Mandel G, Cooperman SS, Maue RA, Goodman RH, Brehm P. Selective induction of brain type II Na^+ channels by nerve growth factor. Proc. Natl. Acad. Sci. USA. 1988; 85:924–928. [PubMed: 2448784]

Massensini AR, Suckling J, Brammer MJ, Moraes-Santos T, Gomez MV, Romano-Silva MA. Tracking sodium channels in live cells: confocal imaging using fluorescently labeled toxins. J. Neurosci. Methods. 2002; 116:189–196. [PubMed: 12044668]

Matsuoka S, Shibata T, Ueda M. Statistical analysis of lateral diffusion and multistate kinetics in single-molecule imaging. Biophys. J. 2009; 97:1115–1124. [PubMed: 19686659]

Maue RA. Understanding ion channel biology using epitope tags: progress, pitfalls, and promise. J. Cell. Physiol. 2007; 213:618–625. [PubMed: 17849449]

Nakada C, Ritchie K, Oba Y, Nakamura M, Hotta Y, Iino R, Kasai RS, Yamaguchi K, Fujiwara T, Kusumi A. Accumulation of anchored proteins forms membrane diffusion barriers during neuronal polarization. Nat. Cell Biol. 2003; 5:626–632. [PubMed: 12819789]

O'Lague PH, Huttner SL, Vandenberg CA, Morrison-Graham K, Horn R. Morphological properties and membrane channels of the growth cones induced in PC12 cells by nerve growth factor. J. Neurosci. Res. 1985; 13:301–321. [PubMed: 2579242]

Qian H, Sheetz MP, Elson EL. Single particle tracking. Analysis of diffusion and flow in two-dimensional systems. Biophys. J. 1991; 60:910–921. [PubMed: 1742458]

Remy S, Beck H, Yaari Y. Plasticity of voltage-gated ion channels in pyramidal cell dendrites. Curr. Opin. Neurobiol. 2010; 20:503–509. [PubMed: 20691582]

Rudy B, Kirschenbaum B, Greene LA. Nerve growth factor-induced increase in saxitoxin binding to rat PC12 pheochromocytoma cells. J. Neurosci. 1982; 2:1405–1411. [PubMed: 7119865]

Scheib H, McLay I, Guex N, Clare JJ, Blaney FE, Dale TJ, Tate SN, Robertson GM. Modeling the pore structure of voltage-gated sodium channels in closed, open, and fast-inactivated conformation reveals details of site 1 toxin and local anesthetic binding. J. Mol. Model. 2006; 12:813–822. [PubMed: 16508760]

Schofield GG, Puhl HL 3rd, Ikeda SR. Properties of wild-type and fluorescent protein-tagged mouse tetrodotoxin-resistant sodium channel (Na V 1.8) heterologously expressed in rat sympathetic neurons. J. Neurophysiol. 2008; 99:1917–1927. [PubMed: 18272876]

Sharonov A, Hochstrasser RM. Wide-field subdiffraction imaging by accumulated binding of diffusing probes. Proc. Natl. Acad. Sci. USA. 2006; 103:18911–18916. [PubMed: 17142314]

Sheetz MP, Wayne DB, Pearlman AL. Extension of filopodia by motor-dependent actin assembly. Cell Motil. Cytoskeleton. 1992; 22:160–169. [PubMed: 1423662]

Strichartz GR, Hall S, Magnani B, Hong CY, Kishi Y, Debin JA. The potencies of synthetic analogues of saxitoxin and the absolute stereoselectivity of decarbamoyl saxitoxin. Toxicon. 1995; 33:723–737. [PubMed: 7676464]

Tikhonov DB, Zhorov BS. Possible roles of exceptionally conserved residues around the selectivity filters of sodium and calcium channels. J. Biol. Chem. 2011; 286:2998–3006. [PubMed: 21081490]

Toledo-Aral JJ, Brehm P, Halegoua S, Mandel G. A single pulse of nerve growth factor triggers long-term neuronal excitability through sodium channel gene induction. Neuron. 1995; 14:607–611. [PubMed: 7695907]

Toledo-Aral JJ, Moss BL, He ZJ, Koszowski AG, Whisenand T, Levinson SR, Wolf JJ, Silos-Santiago I, Halegoua S, Mandel G. Identification of PN1, a predominant voltage-dependent sodium channel expressed principally in peripheral neurons. Proc. Natl. Acad. Sci. USA. 1997; 94:1527–1532. [PubMed: 9037087]

Trimmer JS, Rhodes KJ. Localization of voltage-gated ion channels in mammalian brain. Annu. Rev. Physiol. 2004; 66:477–519. [PubMed: 14977411]

Vaudry D, Stork PJS, Lazarovici P, Eiden LE. Signaling pathways for PC12 cell differentiation: making the right connections. Science. 2002; 296:1648–1649. [PubMed: 12040181]

Vrljic, M.; Nishimura, SY.; Moerner, WE. Single-molecule tracking. Rafts, Lipid, editor. Vol. 398. New Jersey: Humana Press; 2009. p. 193-219.

Wang, H. Tuning DCDHF (dicyanomethylenedihydrofuran) fluorophores and their applications in biological systems. PhD Thesis, Kent State University; 2007.

Zeng S, Tang Y. Effect of clustered ion channels along an unmyelinated axon. Phys. Rev. E Stat. Nonlin. Soft Matter Phys. 2009; 80:021917–021926. [PubMed: 19792161]

Zimmer T, Biskup C, Bollensdorff C, Benndorf K. The β1 subunit but not the β2 subunit colocalizes with the human heart Na^+ channel (hH1) already within the endoplasmic reticulum. J. Membr. Biol. 2002a; 186:13–21. [PubMed: 11891585]

Zimmer T, Biskup C, Dugarmaa S, Vogel F, Steinbis M, Bo¨hle T, Wu YS, Dumaine R, Benndorf K. Functional expression of GFP-linked human heart sodium channel (hH1) and subcellular localization of the a subunit in HEK293 cells and dog cardiac myocytes. J. Membr. Biol. 2002b; 186:1–12. [PubMed: 11891584]

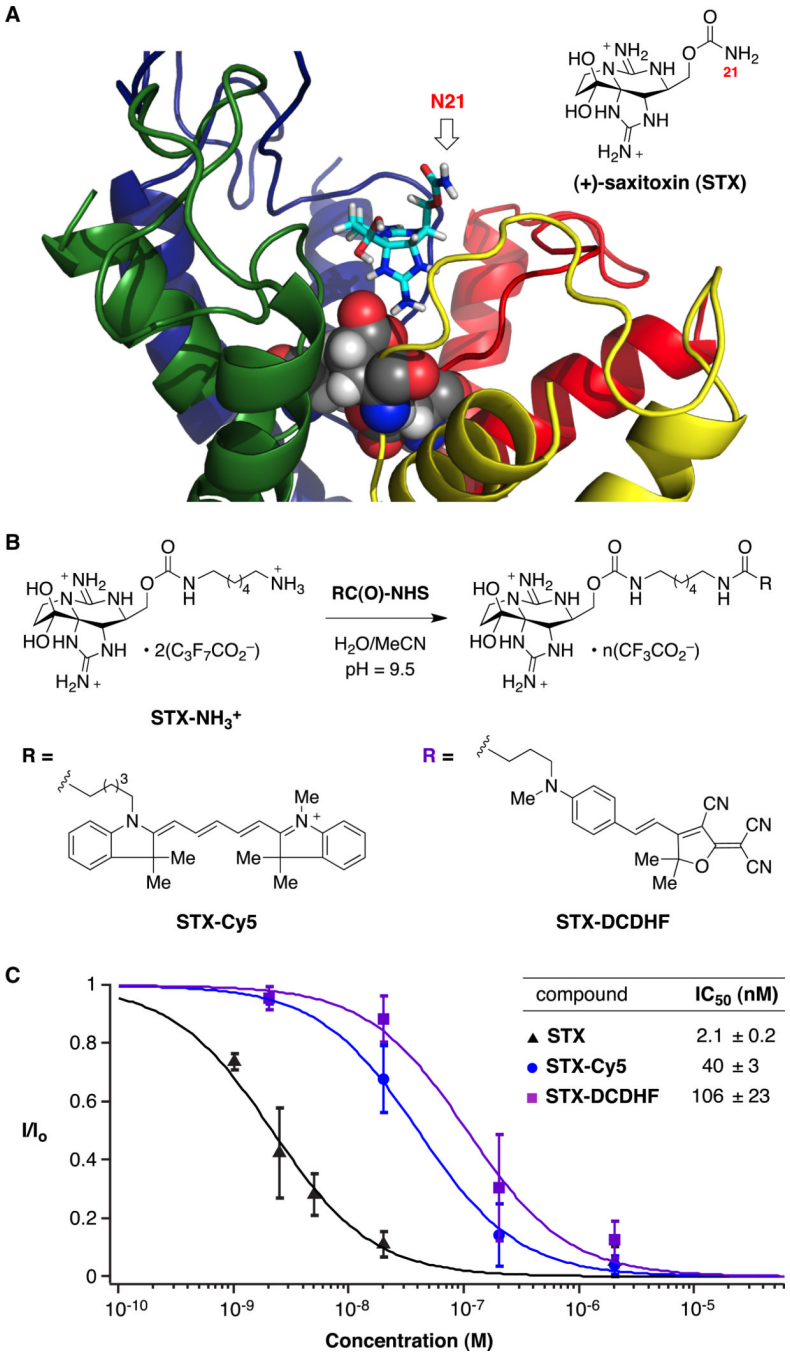

Figure 1. Natural and Synthetic Saxitoxins for Na_V Study

(A) Computational model of STX ligated in the outer mouth of the Na_V pore. The site of STX modification (N21) is indicated by an arrow. Selectivity filter residues (DEKA) are highlighted as space-filling models; domain I = red, domain II = yellow, domain III = green, domain IV = blue.

(B) Synthesis of fluorescent STX derivatives STX-Cy5 and STX-DCDHF from STX-NH_3^+.

(C) Concentration-response curves and IC_{50} values for STX (▲),STX-Cy5(●), and STX-DCDHF (■) on NGF-differentiated PC12 cells (mean ± SD, n = 3).

See also Figures S1, S2, and S3.

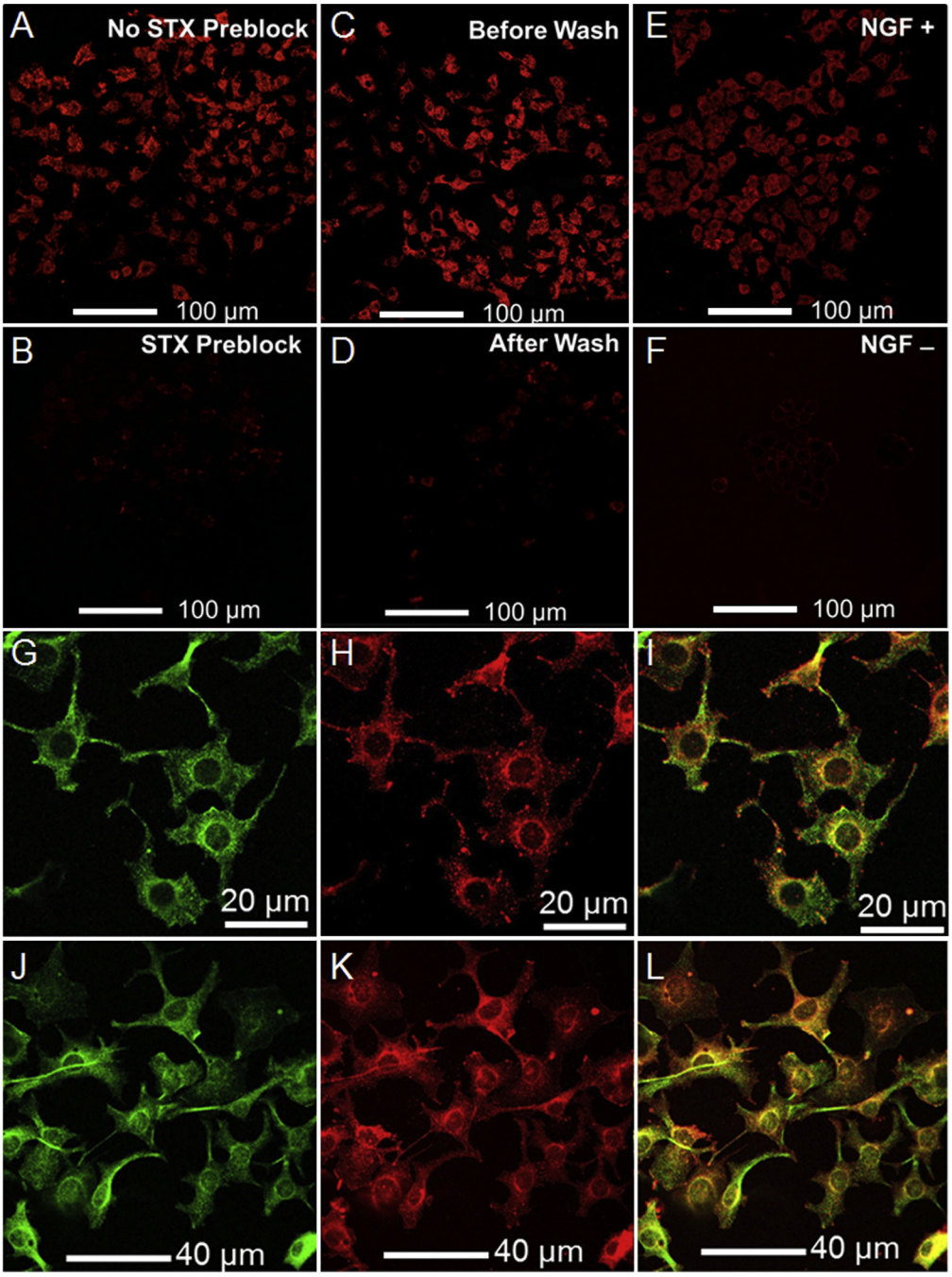

Figure 2. Analysis of Na_V Labeling Using STX-Cy5 and STX-DCDHF in PC12 Cells: Confocal Microscopy Images

Cells were treated with 10 nM STX-Cy5 or 15 nM STX-DCDHF for 15 min prior to imaging.

(A and B) NGF-differentiated PC12 cells in media containing STX-Cy5 following 30 min preincubation in the absence (A) or presence (B) of saturating STX (10 μM), showing preblock of probe fluorescence by STX.

(C and D) NGF-differentiated PC12 cells in media containing STX-Cy5 before (C) and after (D) removal of the probe from the medium, showing fluorescence loss upon probe wash off.

(E and F) NGF-differentiated PC12 cells (E) and undifferentiated PC12 cells (F) in media containing STX-Cy5, showing enhanced fluorescence emission in differentiated cells.
(G and H) NGF-differentiated PC12 cells fixed and exposed to a rat anti-pan Na_V antibody/Alexa488-conjugated secondary antibody (green) (G) then treated with PBS solution containing STX-Cy5 (red) (H).
(I) Merged image of G and H showing visual colocalization. Manders overlap coefficient for STX-Cy5 is 0.94 ± 0.02; STX-DCDHF is 0.93 ± 0.08.
(J–L) Corresponding experiment using STX-DCDHF.
See also Figures S4, S5, and S6.

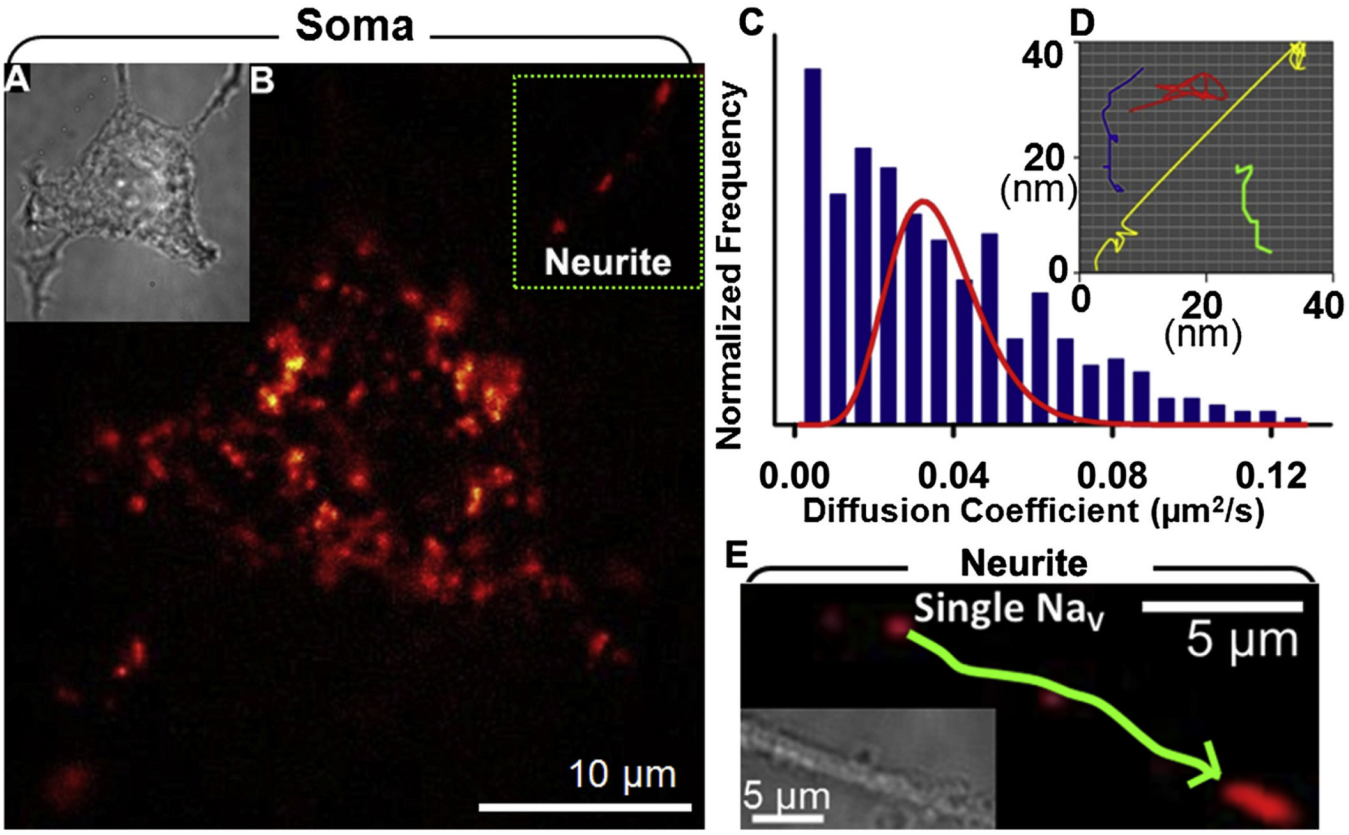

Figure 3. Single Particle Tracking of Na$_V$s in the Soma and Neurites of an NGF-differentiated PC12 Cell: Wide-Field Epifluorescence Microscopy Image

Na$_V$s were labeled with 12.8 nM STX-DCDHF.

(A) Transmission image.

(B) Single 50 ms frame showing individually resolved Na$_V$s in the soma and neurites.

(C) Distribution function for a population of Na$_V$s undergoing Brownian diffusion (solid red line, Davg = 0.036 ± 0.027 µm^2/s, n = 370) superposed on a histogram of measured diffusion coefficients of Na$_V$s in the somatic membrane of the cell in (A).

(D) Representative single-molecule tracks on the soma of the cell in (A).

(E) A long-lived track of a single Na$_V$ in a neurite obtained using low excitation intensity of ~100 W/cm^2. This sample track is comprised of 302 frames acquired at 50 ms exposure (blue line) superposed on a single frame image containing the tracked molecule (green arrow). Trajectories in neurites yield instantaneous velocities of 680–970 ±10 nm/s (n = 5).

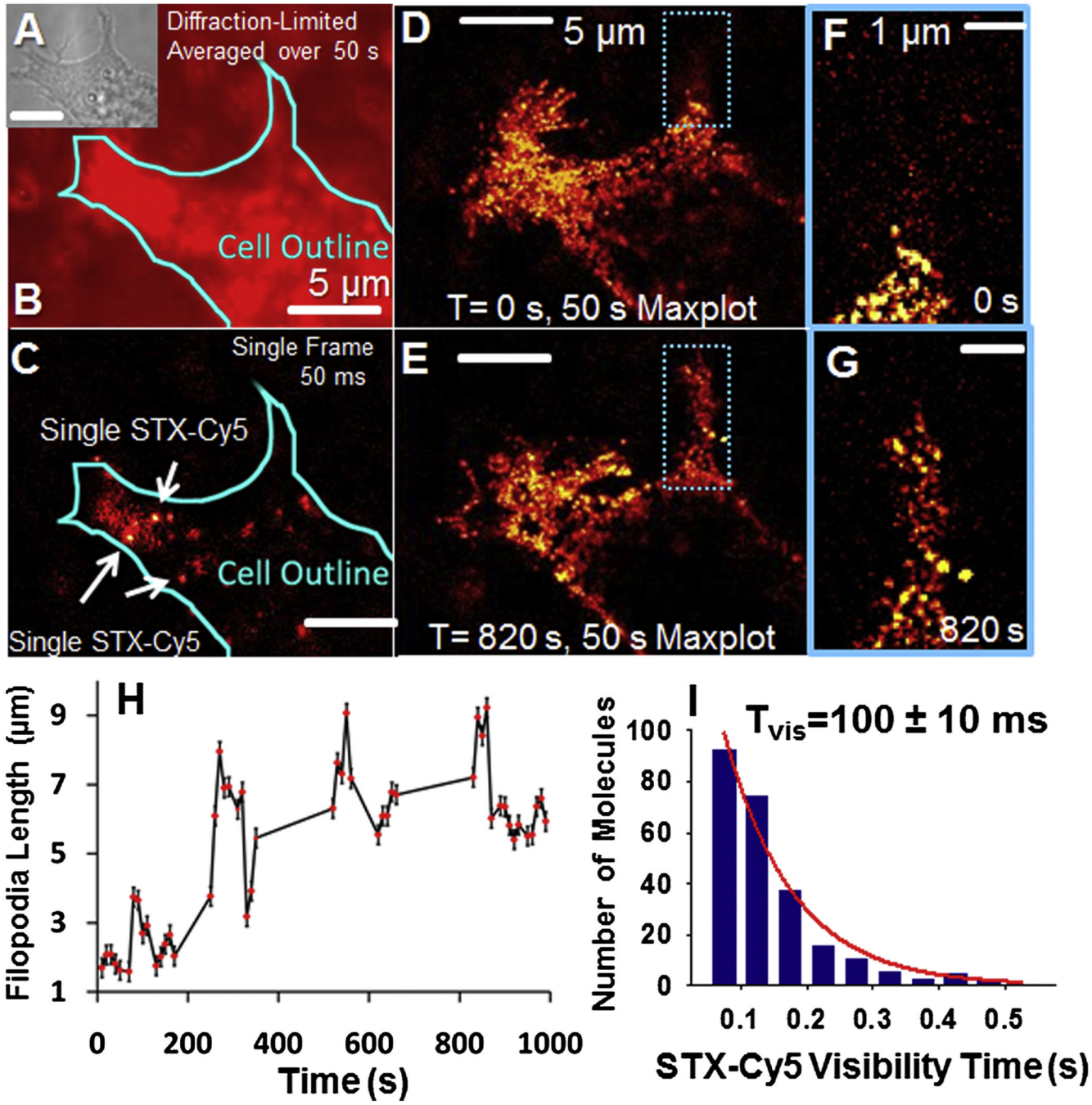

Figure 4. Single-Molecule Imaging of Na_Vs in Filopodia of an NGF-Differentiated PC12 Cell: Wide-Field Epifluorescence Microscopy Image

Na_Vs were labeled with 3 nM STX-Cy5.

(A) Transmission image.

(B) Diffraction-limited image of (A) averaged over 50 s.

(C) Single 50 ms frame with labeled Na_Vs resolved as single molecules.

(D) A 50 s fluorescence maxplot of the cell in (A) at t = 0 highlighting the base of an extending filopodium (blue box).

(E) A 50 s fluorescence maxplot of the cell in (A) at t = 820 s showing elongation of the highlighted filopodium.

(F) Magnified image of the boxed area in (D).
(G) Magnified image of the boxed area in (E).
(H) Length of the filopodium highlighted in (D–G)
plotted as a function of time (mean ± 2 × SD, n = 3).
(I) Visibility time of STX-Cy5 on the membrane of the cell in (A) at 200 W/cm^2 intensity
(average T_{vis} = 100 ± 10 ms).
See also Figures S7 and S8.

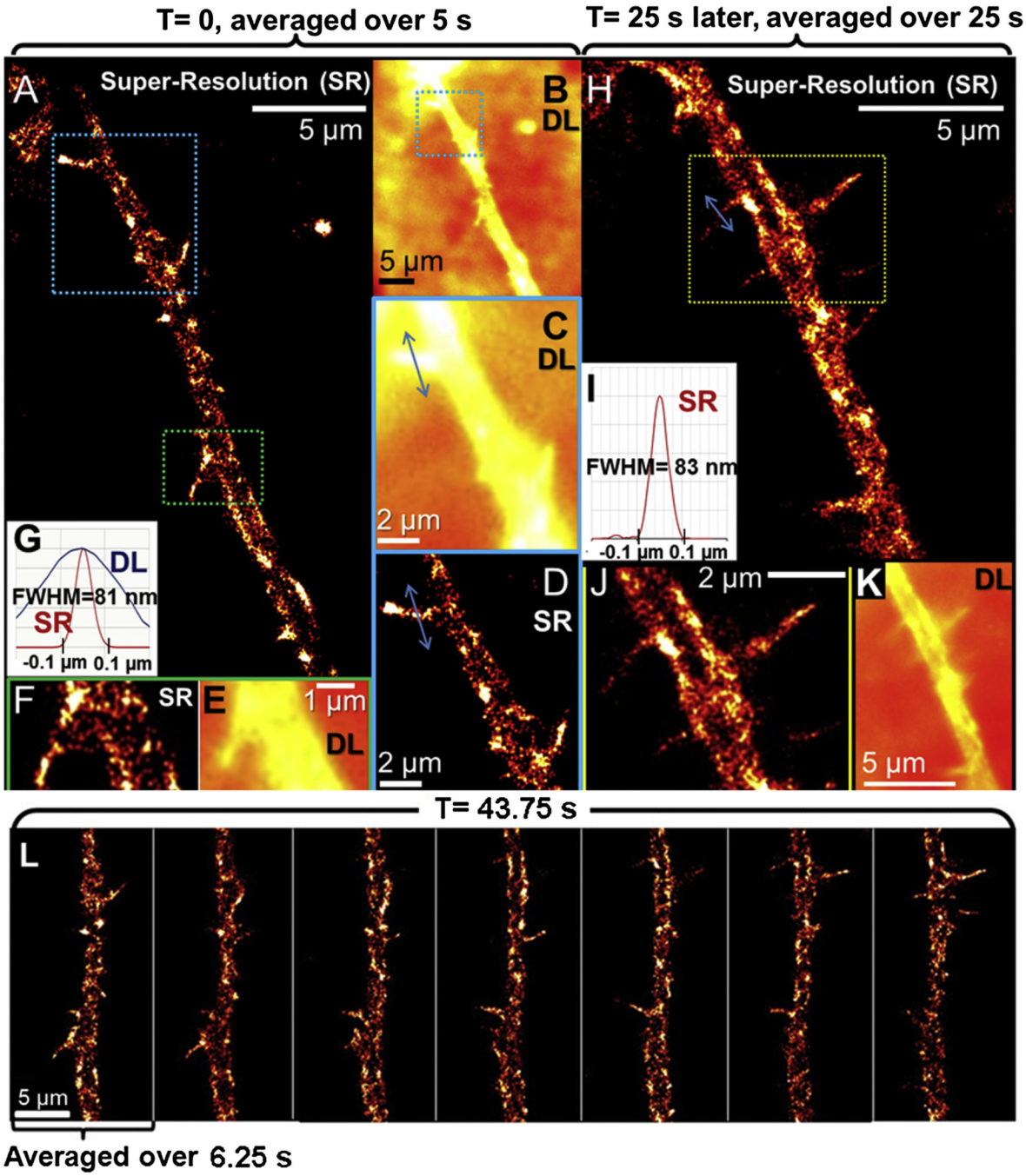

Figure 5. Super-Resolution Imaging of Na_Vs in Neuritic Spines of an NGF-Differentiated PC12 Cell

Na_Vs were labeled with 10 nM STX-Cy5.

(A) Super-resolution image acquired over 5 s at a 50 ms frame rate.

(B) Diffraction-limited image of (A).

(C) Diffraction-limited image of the blue boxed area in (A).

(D) Super-resolution image of the blue boxed area in (A).

(E) Diffraction-limited image of the green boxed area in (A).

(F) Super-resolution image of the green boxed area in (A).

(G) Measured full width at half maximum (FWHM) values for the neuritic spine indicated by the blue arrow in (E) and (F) from diffraction-limited (400 nm, blue line) and super-resolution (81 nm, red line) images.
(H) Super-resolution image of (A) 25 s later, acquired over 25 s at a 50 ms frame rate.
(I) Measured FWHM value for the super-resolved neuritic spine indicated by the blue arrow in (H).
(J) Super-resolution image of the yellow boxed area in (H).
(K) Diffraction-limited image of the yellow boxed area in (H).
(L) Sequence of frames showing dynamic behavior of the neuritic spines. DL, diffraction-limited; SR, super-resolution.
See also Figure S8 and Movie S1.